appears to be an extensive variable (i.e., one that grows linearly with the system size). These variables are nonextensive in the randomized networks. The existence of such variables may be a unifying property of evolved or designed systems. The decrease of the concentration C with randomized network size S (Fig. 3) qualitatively agrees with exact results (*2*, *26*) on Erdos-Renyi random graphs (random graphs that preserve only the number of nodes and edges of the real network) in which $C \sim 1/S$. In general, the larger the network is, the more significant the motifs tend to become. This trend can also be seen in Table 1 by comparing networks of different sizes. The network motif detection algorithm appears to be effective even for rather small networks (on the order of 100 edges). This is because three- or four-node subgraphs occur in large numbers even in small networks. Furthermore, our approach is not sensitive to data errors; for example, the sets of significant network motifs do not change in any of the networks upon addition, removal, or rearrangement of 20% of the edges at random.

In information-processing networks, the motifs may have specific functions as elementary computational circuits (*11*). More generally, they may be interpreted as structures that arise because of the special constraints under which the network has evolved (*27*). It is of value to detect and understand network motifs in order to gain insight into their dynamical behavior and to define classes of networks and network homologies. Our approach can be readily generalized to any type of network, including those with multiple "colors" of edges or nodes. It would be fascinating to see what types of motifs occur in other networks and to understand the processes that yield given motifs during network evolution.

References and Notes

1. S. H. Strogatz, *Nature* **410**, 268 (2001).
2. B. Bollobas, *Random Graphs* (Academic, London, 1985).
3. D. Watts, S. Strogatz, *Nature* **393**, 440 (1998).
4. A.-L. Barabási, R. Albert, *Science* **286**, 509 (1999).
5. M. Newman, *Proc. Natl. Acad. Sci. U.S.A.* **98**, 404 (2001).
6. H. Jeong, B. Tombor, R. Albert, Z. N. Oltvai, A. L. Barabasi, *Nature* **407**, 651 (2000).
7. R. F. Cancho, C. Janssen, R. V. Sole, *Phys. Rev. E* **64**, 046119 (2001).
8. R. F. Cancho, R. V. Sole, *Proc. R. Soc. London Ser. B* **268**, 2261 (2001).
9. L. Amaral, A. Scala, M. Barthelemy, H. Stanley, *Proc. Natl. Acad. Sci. U.S.A.* **97**, 11149 (2000).
10. B. Huberman, L. Adamic, *Nature* **401**, 131 (1999).
11. S. Shen-Orr, R. Milo, S. Mangan, U. Alon, *Nature Genet.* **31**, 64 (2002).
12. P. Holland, S. Leinhardt, in *Sociological Methodology*, D. Heise, Ed. (Jossey-Bass, San Francisco, 1975), pp. 1–45.
13. S. Wasserman, K. Faust, *Social Network Analysis* (Cambridge Univ. Press, New York, 1994).
14. N. Guelzim, S. Bottani, P. Bourgine, F. Kepes, *Nature Genet.* **31**, 60 (2002).
15. M. Newman, S. Strogatz, D. Watts, *Phys. Rev. E* **64**, 6118 (2001).
16. S. Maslov, K. Sneppen, *Science* **296**, 910 (2002).
17. The randomized networks used for detecting three-node motifs preserve the numbers of incoming, outgoing, and double edges with both incoming and outgoing arrows for each node. The randomized networks used for detecting four-node motifs preserve the above characteristics as well as the numbers of all 13 three-node subgraphs as in the real network. Algorithms for constructing these randomized network ensembles are described (*18*). Additional information is available at www.weizmann.ac.il/mcb/UriAlon.
18. Methods are available as supporting material on *Science* Online.
19. D. Thieffry, A. M. Huerta, E. Perez-Rueda, J. Collado-Vides, *Bioessays* **20**, 433 (1998).
20. M. C. Costanzo *et al.*, *Nucleic Acids Res.* **29**, 75 (2001).
21. J. Cohen, F. Briand, C. Newman, *Community Food Webs: Data and Theory* (Springer, Berlin, 1990).
22. R. Williams, N. Martinez, *Nature* **404**, 180 (2000).
23. S. Pimm, J. Lawton, J. Cohen, *Nature* **350**, 669 (1991).
24. J. White, E. Southgate, J. Thomson, S. Brenner, *Philos. Trans. R. Soc. London Ser. B* **314**, 1 (1986).
25. F. Brglez, D. Bryan, K. Kozminski, *Proc. IEEE Int. Symp. Circuits Syst.*, 1929 (1989).
26. In Erdos-Renyi randomized networks with a fixed connectivity (*2*), the concentration of a subgraph with n nodes and k edges scales with network size as $C \sim S^{n-k-1}$ (thus, $C \sim 1/S$ for the feedforward loop of Fig. 3 where $n = k = 3$). The sole exception in Table 1 in which C should not vanish at large S is the three-chain pattern in food webs where $n = 3$ and $k = 2$.
27. D. Callaway, J. Hopcroft, J. Kleinberg, M. Newman, S. Strogatz, *Phys. Rev. E* **64**, 041902 (2001).

28. We thank S. Maslov and K. Sneppen for valuable discussions. We thank J. Collado-Vides, N. Martinez, R. Govindan, R. Durbin, L. Amaral, R. Cancho, S. Maslov, and K. Sneppen for kindly providing data, as well as D. Alon, E. Domany, M. Elowitz, I. Kanter, O. Hobart, M. Naor, D. Mukamel, A. Murray, S. Quake, R. Raz, M. Reigl, M. Surette, K. Sneppen, P. Sternberg, E. Winfree, and all members of our lab for comments. We thank Caltech and the Aspen Center for Physics for their hospitality during part of this work. We acknowledge support from the Israel Science Foundation, the Human Frontier Science Program, and the Minerva Foundation.

Supporting Online Material

www.sciencemag.org/cgi/content/full/298/5594/824/DC1
Methods
Table S1

1 May 2002; accepted 10 September 2002

Progression of Vertebrate Limb Development Through SHH-Mediated Counteraction of GLI3

Pascal te Welscher,[1] Aimée Zuniga,[1] Sanne Kuijper,[2] Thijs Drenth,[1] Hans J. Goedemans,[1] Frits Meijlink,[2] Rolf Zeller[1]*

Distal limb development and specification of digit identities in tetrapods are under the control of a mesenchymal organizer called the polarizing region. *Sonic Hedgehog* (SHH) is the morphogenetic signal produced by the polarizing region in the posterior limb bud. Ectopic anterior SHH signaling induces digit duplications and has been suspected as a major cause underlying congenital malformations that result in digit polydactyly. Here, we report that the polydactyly of *Gli3*-deficient mice arises independently of SHH signaling. Disruption of one or both *Gli3* alleles in mouse embryos lacking *Shh* progressively restores limb distal development and digit formation. Our genetic analysis indicates that SHH signaling counteracts GLI3-mediated repression of key regulator genes, cell survival, and distal progression of limb bud development.

The *Hedgehog* (*Hh*) signaling pathway controls many key developmental processes during animal embryogenesis (*1*). In *Drosophila* embryos, all known functions of Hh signaling are mediated by the transcriptional effector Cubitus interruptus (Ci) (*2*). Several homologs of *Hh* and *Ci* have been identified in higher vertebrates. In particular, *Sonic Hedgehog* (SHH) and the *Ci* homolog GLI3 are required for vertebrate limb development (*3*–*6*). GLI3 acts first during the initiation of limb bud development and before the activation of SHH signaling in posterior restriction of the basic helix-loop-helix transcription factor dHAND. dHAND in turn prevents *Gli3* expression from spreading posteriorly (Fig. 1A, panel 1) (*7*). In addition, GLI3 restricts the SHH-independent early expression of *5′HoxD* genes and *Gremlin* to the posterior mesenchyme (*8*). Subsequently, dHAND functions in the activation of *Shh* expression (*9*). Limb bud morphogenesis is then controlled by reciprocal interactions of two signaling centers (Fig. 1A, panel 2): the polarizing region, an instructive organizer located in the posterior limb bud mesenchyme, and the apical ectodermal ridge (AER). SHH signaling by the polarizing region in combination with bone morphogenetic proteins

[1]Department of Developmental Biology, Faculty of Biology, Utrecht University, Padualaan 8, NL-3584 CH Utrecht, Netherlands. [2]Hubrecht Laboratorium, Uppsalalaan 8, NL-3584 CT Utrecht, Netherlands.

*To whom correspondence should be addressed. E-mail: R.Zeller@bio.uu.nl

(BMPs) and their antagonists instruct limb skeletal patterning, most likely by regulating the expression of 5′HoxD transcription factors (Fig. 1A, panel 2) (*10*, *11*). The BMP antagonist *Gremlin* mediates a signal relay from the polarizing region to the AER (*12*), and fibroblast growth factor (FGF) signaling by the AER maintains the polarizing region to enable progression of limb bud morphogenesis (SHH-FGF feedback loop) (*10*, *11*).

Ectopic anterior expression of SHH in limb buds induces digit duplications, and this ectopic expression is viewed as a major cause of limb polydactylous (extra digits) phenotypes (*10*, *11*). Spontaneous mutations affecting GLI3 cause a severe congenital malformation in mice [Extra-toes (Xt)] (*3*, *13*) and several related syndromes in humans (*14*). The associated polydactylous phenotypes have so far been attributed to ectopic *Shh* expression (*13*) and anteriorly expanded *5′Hoxd* expression (*8*). In the absence of SHH signaling, full-length GLI3 is proteolytically cleaved to a smaller protein (GLI3-83) (*15*). Such truncated forms of GLI3 protein have repressor activity (*16*, *17*). However, SHH signaling inhibits GLI3 processing, which may allow the full-length protein to function as a transcriptional activator (*18*, *19*). Biochemical analysis showed that long-range SHH signaling and inhibition of GLI3 processing in limb buds (Fig. 1A, panel 2) result in formation of an anterior-to-posterior graded distribution (high to low) of the truncated GLI3-83 protein with repressor activity (*15*).

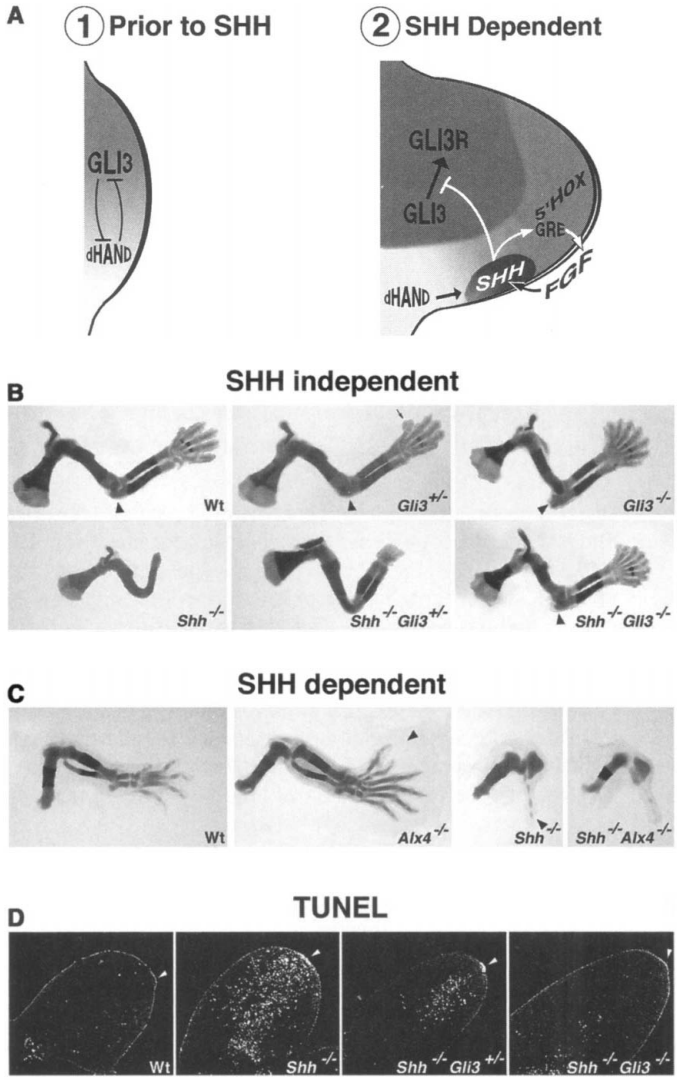

Fig. 1. (**A**) Interactions of key regulators of vertebrate limb development: ① Reciprocal antagonism of GLI3 and dHAND prepatterns the limb bud mesenchyme before activation of SHH signaling. ② dHAND is required to activate *Shh* expression by polarizing region cells. SHH signaling inhibits the processing of GLI3 to GLI3-83, which acts as transcriptional repressor (GLI3R). SHH positively regulates *5′HoxD* (*5′HOX*) gene and *Gremlin* (GRE) expression in distal mesenchyme. The SHH-FGF feedback loop between the polarizing region and the AER is established through Gremlin-mediated BMP antagonism. Only the interactions relevant to the present study are shown. (**B**) Skeletal stains of forelimbs [embryonic day 16.5 (E16.5)] of *Shh* and *Gli3* single- and double-mutant mouse embryos (*28*). Arrowheads point to well-formed elbow joints. Genotype labels: Wt, wild-type; $Gli3^{+/-}$, one allele of *Gli3* inactivated, arrow points to small ectopic cartilage condensation; $Gli3^{-/-}$, *Gli3*-deficient; $Shh^{-/-}$, *Shh*-deficient; $Shh^{-/-}$, $Gli3^{+/-}$, $Shh^{-/-}$ lacking in addition one functional *Gli3* allele; $Shh^{-/-}$, $Gli3^{-/-}$, forelimb of a double-homozygous embryo. (**C**) Skeletal stains of hindlimbs (E14.5) of *Shh* and *Alx4* single- and double-mutant mouse embryos. Genotype labels: $Alx4^{-/-}$, *Alx4* deficient, arrowhead points to a duplicated preaxial digit 2 (phenotype is 100% penetrant in hindlimbs); $Shh^{-/-}$, arrowhead points to the one digit formed; $Shh^{-/-}$, $Alx4^{-/-}$, hindlimb of a double homozygous embryo. (**D**) Detection of apoptotic cells (*29*) in forelimb buds of $Shh^{-/-}$ embryos (E10.75, 38 to 39 somites) lacking one or both *Gli3* alleles. Shown are representative sections at similar levels (anterior-dorsal is to the left and posterior-ventral is to the right). Anterior is to the top and posterior to the bottom in all panels. Arrowheads point to the AER. TUNEL, terminal deoxynucleotidyl transferase–mediated deoxyuridine triphosphate nick-end labeling.

To identify the essential function(s) and to study the phenotypic consequences of these GLI3-SHH interactions, we analyzed the limb development of *Shh* and *Gli3* double-mutant embryos (*20*) (Fig. 1B). The limbs of *Gli3*-deficient ($Gli3^{-/-}$) embryos are polydactylous (Fig. 1B) (*13*), whereas one fused forearm (zeugopod) bone and no digit arch (autopod) form in limbs of *Shh*-deficient ($Shh^{-/-}$) embryos (Fig. 1B) (*5*, *6*). Disruption of one *Gli3* allele in *Shh*-deficient ($Shh^{-/-}$, $Gli3^{+/-}$) embryos improves distal limb development, as two zeugopodal bones and rudimentary digits form (Fig. 1B). The limbs of double-homozygous ($Shh^{-/-}$, $Gli3^{-/-}$) mouse embryos are gross-morphologically indistinguishable from the limbs of $Gli3^{-/-}$ embryos (Fig. 1B and fig. S1). This genetic analysis establishes that the polydactylous limb phenotype of *Gli3*-deficient embryos is not caused by ectopic SHH signaling as previously assumed (*13*). Another molecularly well-studied mouse mutation with a polydactylous phenotype is Strong's Luxoid (Lst), which is caused by disruption of the transcription factor Alx4 ($Alx4^{-/-}$, Fig. 1C) (*21*). In wild-type limb buds, *Alx4* is expressed in the anterior mesenchyme, and a functional anterior SHH signaling center is established in the limb buds of $Alx4^{-/-}$ embryos that is similar to the one in $Gli3^{-/-}$ embryos. In contrast to *Gli3*, no rescue of distal limb development is observed in limbs lacking *Shh* and *Alx4* (Fig. 1C) (*20*). These results establish that two different mechanisms can cause polydactyly. The polydactyly of $Alx4^{-/-}$ mice depends on SHH signaling, whereas the polydactyly of $Gli3^{-/-}$ mice is SHH independent. The limb phenotype of $Gli3^{-/-}$ mouse embryos is similar to that of talpid chicken embryos (*22*). Biochemical evidence shows that GLI3-83 repressor levels are substantially reduced in talpid mutant embryos (*15*), which indicates that this polydactyly may also occur independent of SHH signaling (*22*).

The results shown in Fig. 1B reveal that SHH-independent restoration of distal limb development in $Shh^{-/-}$ embryos is *Gli3*-dose dependent. Because massive cell death occurs in limb buds of $Shh^{-/-}$ embryos (Fig. 1D) (*5*), the progressive restoration of distal limb development (Fig. 1A) may be due to improved cell survival. Indeed, apoptosis is reduced in limb buds of $Shh^{-/-}$ embryos lacking one functional *Gli3* allele but is still higher than apotosis in wild types (Fig. 1D). The low levels of apoptotic cells in limb buds of double homozygous embryos are, however, comparable to the levels in wild-type (Fig. 1D) and *Gli3*-deficient embryos (*23*).

To exclude the possibility that ligand-independent activation of intracellular SHH signal transduction restores limb development in *Shh* and *Gli3* double mutant embryos (Fig. 1B), we analyzed the expression of the SHH tran-

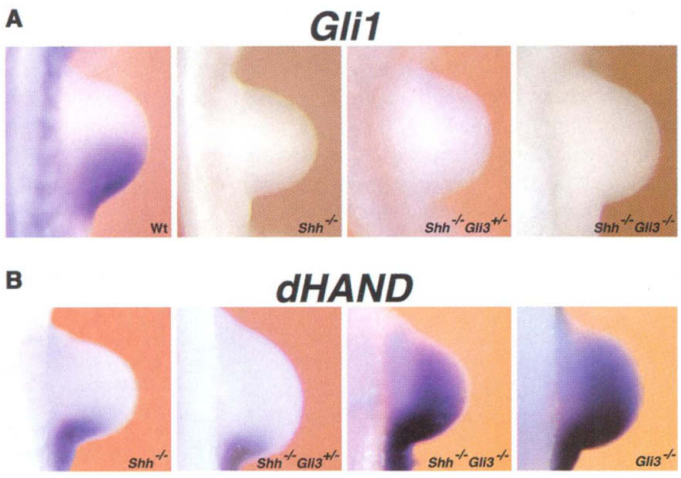

Fig. 2. Expression of *Gli1* (**A**) and *dHAND* (**B**) in limb buds of *Shh* and *Gli3* single- and double-mutant embryos at E10.25 (32 to 33 somites). All limb buds are oriented with anterior to the top and posterior to the bottom. Genotypes are as described in Fig. 1B.

scriptional targets *Patched* (*Ptc*) and *Gli1* (*11*, *24*). Neither *Ptc* (*23*) nor *Gli1* were expressed in the limb buds of $Shh^{-/-}$ embryos lacking either one or both *Gli3* alleles (Fig. 2A). The *Gli3* dose-dependent improvement of limb development is also not linked to alterations of *dHAND*, because its expression remains posteriorly restricted in limb buds of $Shh^{-/-}$, $Gli3^{+/-}$ embryos (Fig. 2B). The disruption of both *Gli3* alleles results in SHH-independent anterior *dHAND* expression during early limb development (Fig. 2B) (*7*).

The SHH-FGF feedback loop is established through *Gremlin*-mediated BMP antagonism (Fig. 1A, panel 2). *Gremlin* and *Fgf4* expression are activated but not maintained in limb buds of $Shh^{-/-}$ embryos (Fig. 3) (*12*). Low

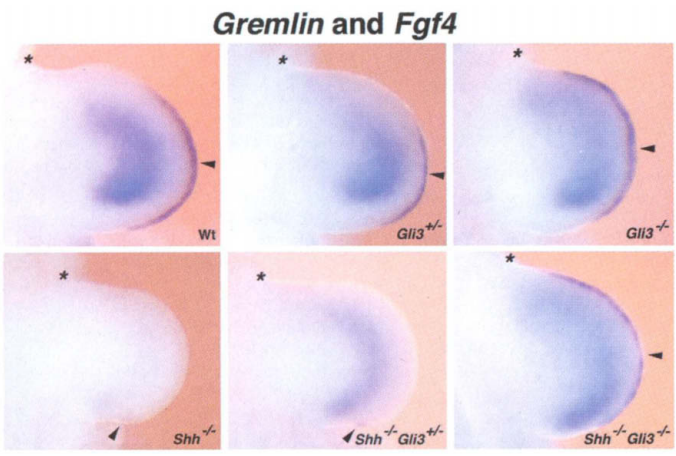

Fig. 3. (**Left**) Differential rescue of *Gremlin* expression in the limb bud mesenchyme and *Fgf4* in the AER. *Gremlin* (mesenchyme) and *Fgf4* (AER) in limb buds (E 10.75, 37 to 38 somites) are simultaneously detected. Asterisks indicate anterior margin of the limb buds. Arrowheads point to *Fgf4* expression in the AER. Genotypes are as described in Fig. 1B.

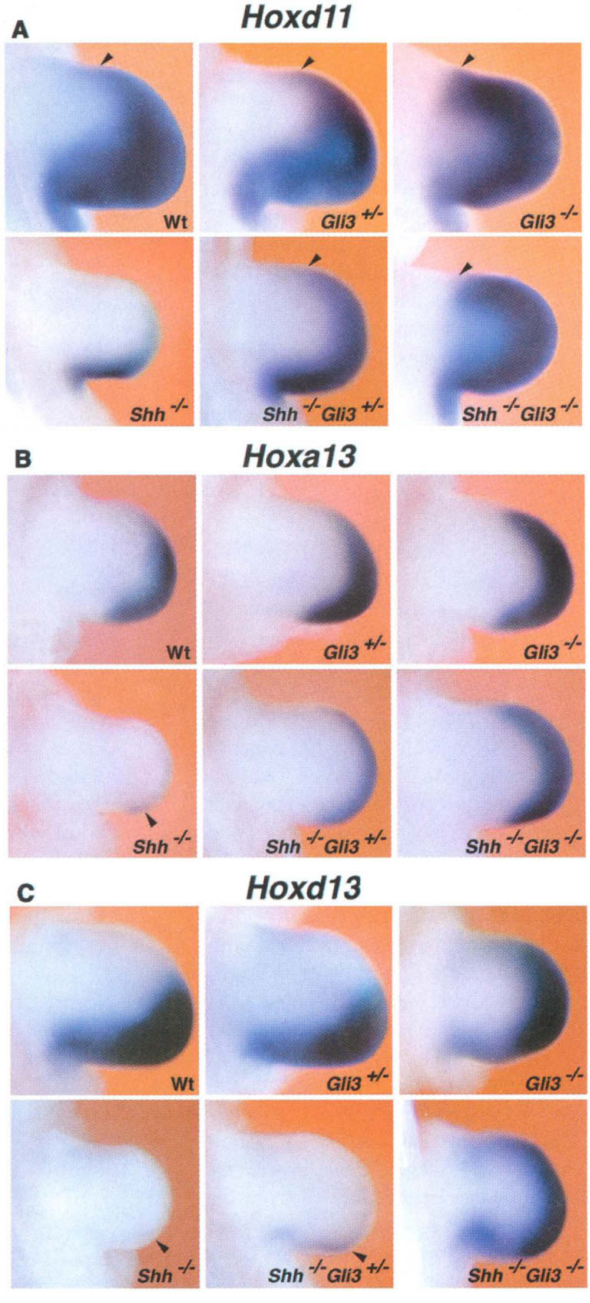

Fig. 4. (**Right**) *Gli3* dose-dependent up-regulation of 5′HoxD and 5′HoxA expression in limb buds of $Shh^{-/-}$ embryos. All limb buds (E 10.75, 37 to 38 somites) are oriented with anterior to the top and posterior to the bottom. (**A**) Expression of *Hoxd11*. Arrowheads indicate the anterior expression boundary. (**B**) Expression of *Hoxa13*. (**C**) Expression of *Hoxd13*. Arrowheads in (B) and (C) indicate low expression of respective gene. Genotypes are as described in Fig. 1B.

levels of *Gremlin* but not *Fgf4* transcripts are detected in limb buds of $Shh^{-/-}$ embryos lacking one *Gli3* allele (Fig. 3). In double-homozygous embryos, *Gremlin* and *Fgf4* expression in limb buds is comparable to that in $Gli3^{-/-}$ embryos. The differential restoration of *Fgf4* indicates that its induction may depend on a threshold of BMP antagonism.

Hoxa11 and Hoxd11 are essential to pattern the zeugopod, whereas Hoxa13 and Hoxd13 are essential for autopod patterning (*25*). In $Shh^{-/-}$ limb buds, *Hoxa11* remains expressed (*23*), whereas *Hoxd11* is rapidly down-regulated (Fig. 4A). The disruption of one *Gli3* allele in $Shh^{-/-}$ embryos partially restores *Hoxd11* expression such that its anterior boundary in limb buds is located at a position similar to that in wild type (arrowheads, Fig. 4A). This restoration provides a likely molecular explanation for improved zeugopod development in $Shh^{-/-}$, $Gli3^{+/-}$ embryos (Fig. 1B). The expressions of both *Hoxa13* and *Hoxd13* are low in limb buds of $Shh^{-/-}$ embryos (Fig. 4, B and C) (*4*–*6*). The additional inactivation of one *Gli3* allele restores *Hoxa13* expression to intermediate levels (Fig. 4B), whereas *Hoxd13* transcripts remain low (arrowhead, Fig. 4C). In limb buds of double homozygous embryos, all three *5′Hox* genes are expressed at levels similar to those expressed in $Gli3^{-/-}$ embryos (Fig. 4, A to C). These results indicate that the progressive restoration of distal limb development (Fig. 1B) is likely due to *Gli3* dose-dependent restoration of the distal *5′Hoxa* and distal *5′Hoxd* expression domains in limb buds of $Shh^{-/-}$ embryos.

Our study provides genetic evidence for an important sequential interaction of GLI3 with dHAND and SHH. The SHH-independent nature of the digit polydactyly in $Gli3^{-/-}$ limb buds is most likely a direct consequence of the early anterior expansion of the expression of "posterior" genes such as *5′Hoxd* genes (*7*, *8*). The scapula and stylopod (not affected in $Shh^{-/-}$ embryos) (*5*, *6*) may be patterned by the genetic interaction of *GLI3* with *dHAND* before the activation of SHH signaling (Fig. 1A, panel 1) (*7*). In limb buds of $Shh^{-/-}$ embryos, *Gli3* expression expands posteriorly, concurrent with the down-regulation of "posterior" genes and the onset of apoptosis (*5*, *6*, *12*), which cause the "shut-down" of distal limb development and antero-posterior patterning. The *Gli3*-dose-dependent restoration of cell survival and limb bud development in $Shh^{-/-}$ embryos indicates that, in wild-type limb buds, SHH counteracts GLI3 to enable progression of outgrowth and patterning. The polarizing region is propagated distally, and SHH signaling is up-regulated via the SHH-FGF feedback loop (Fig. 1A, panel 2) (*11*, *12*). Such up-regulation of SHH signaling should increasingly inhibit GLI3 processing and should result in a graded GLI3-83 repressor distribution as shown biochemically (*15*). The resulting full-length GLI3 protein may also function in positive transcriptional regulation of SHH targets (*18*, *19*). Although the SHH-GLI3 interactions enable distal limb development and formation of a digit arch, additional signals such as BMPs participate in specification of digit identities (*26*). Lastly, aspects of the dorso-ventral neural tube patterning (disrupted in $Shh^{-/-}$ embryos) are also restored in mouse embryos mutant for both *Shh* and *Gli3* (*27*). This shows that regulation of GLI3 by SHH signaling (and vice versa) is of general functional importance during embryonic development.

References and Notes

1. P. W. Ingham, A. P. McMahon, *Genes Dev.* **15**, 3059 (2001).
2. N. Methot, K. Basler, *Development* **128**, 733 (2001).
3. C. Hui, A. Joyner, *Nature Genet.* **3**, 241 (1993).
4. C. Chiang *et al.*, *Nature* **383**, 407 (1996).
5. C. Chiang *et al.*, *Dev. Biol.* **236**, 421 (2001).
6. P. Kraus, D. Fraidenraich, C. A. Loomis, *Mech. Dev.* **100**, 45 (2001).
7. P. te Welscher, M. Fernandez-Teran, M. A. Ros, R. Zeller, *Genes. Dev.* **16**, 421 (2002).
8. A. Zuniga, R. Zeller, *Development* **126**, 13 (1999).
9. M. J. Cohn, *Nature* **406**, 953 (2000).
10. R. L. Johnson, C. J. Tabin, *Cell* **90**, 979 (1997).
11. J. Capdevila, J. C. Izpisua Belmonte, *Annu. Rev. Cell Dev. Biol.* **17**, 87 (2001).
12. A. Zuniga, A. P. Haramis, A. P. McMahon, R. Zeller, *Nature* **401**, 598 (1999).
13. H. Masuya, T. Sagai, S. Wakana, K. Moriwaki, T. Shiroishi, *Genes Dev.* **9**, 1645 (1995).
14. L. Biesecker, *Nature Genet.* **17**, 259 (1997).
15. B. Wang, J. F. Fallon, P. A. Beachy, *Cell* **100**, 423 (2000).
16. S. H. Shin, P. Kogerman, E. Lindstrom, R. Toftgard, L. G. Biesecker, *Proc. Natl. Acad. Sci. U.S.A.* **96**, 2880 (1999).
17. A. Ruiz i Altaba, *Development* **126**, 3205 (1999).
18. P. Dai *et al.*, *J. Biol. Chem.* **274**, 8143 (1999).
19. R. Brewster, J. L. Mullor, A. Ruiz i Altaba, *Development* **127**, 4395 (2000).
20. $Shh^{-/-}$ embryos, the Lst^{J} (inactivated *Alx4*) and Xt^{J} (inactivated *Gli3*) mouse strains (superscript *J* indicates *Jackson* alleles), were used and genotyped as described (*3*, *6*, *21*).
21. S. Qu *et al.*, *Development* **125**, 2711 (1998).
22. N. C. Caruccio *et al.*, *Dev. Biol.* **212**, 137 (1999).
23. P. te Welscher *et al.*, data not shown.
24. R. L. Johnson, R. D. Riddle, C. J. Tabin, *Curr. Opin. Genet. Dev.* **4**, 535 (1994).
25. J. Zakany, D. Duboule, *Cell Tissue Res.* **296**, 19 (1999).
26. G. Drossopoulou *et al.*, *Development* **127**, 1337 (2000).
27. Y. Litingtung, C. Chiang, *Nature Neurosci.* **3**, 979 (2000).
28. Embryos were stained for cartilage and bones with the use of combined Alcian blue and Alizarin red coloring.
29. Apoptotic cells were detected by incorporating fluorescein–deoxyuridine 5′-triphosphate into fragmented DNA using terminal transferase (Roche Diagnostics, Mannheim, Germany).

30. We thank J. Deschamps, R. Dono, G. Holländer, R. Plasterk, B. Scheres, D. Welch, and group members for comments and suggestions. A.Z. is a fellow of the Royal Netherlands Academy of Arts and Sciences. Supported by the Netherlands Research Organization (program grant 810.68.012/3 to F.M. and R.Z.).

Supporting Online Material
www.sciencemag.org/cgi/content/full/1075620/DC1
Fig. S1

1 July 2002; accepted 22 August 2002
Published online 5 September 2002;
10.1126/science.1075620
Include this information when citing this paper.

Timing Requirements for Insulin/IGF-1 Signaling in *C. elegans*

Andrew Dillin,* Douglas K. Crawford, Cynthia Kenyon†

The insulin/IGF-1 (where IGF-1 is insulin-like growth factor–1) signaling pathway influences longevity, reproduction, and diapause in many organisms. Because of the fundamental importance of this system in animal physiology, we asked when during the animal's life it is required to regulate these different processes. We find that in *Caenorhabditis elegans*, the pathway acts during adulthood, to relatively advanced ages, to influence aging. In contrast, it regulates diapause during development. In addition, the pathway controls longevity and reproduction independently of one another. Together our findings show that life-span regulation can be dissociated temporally from phenotypes that might seem to decrease the quality of life.

In *C. elegans*, mutations that decrease the activity of DAF-2, an insulin/IGF-1-like receptor, or downstream phosphatidylinositol 3-kinase, phosphoinositide-dependent kinase, or AKT (also known as protein kinase B) signaling components prolong youthfulness and double the life-span of the animal. The DAF-2 pathway influences other processes as well. All *daf-2* examined mutations increase resistance to oxidative stress and delay reproduction (some alleles also reduce fertility). Strong *daf-2* mutations cause juvenile animals to enter a state of diapause, called dauer, instead of growing to adulthood. All of these mutant phenotypes re-

Department of Biochemistry and Biophysics, University of California, San Francisco, San Francisco, CA 94143–0448, USA.

*Present address: Molecular and Cell Biology Laboratory, The Salk Institute for Biological Studies, La Jolla, CA 92037, USA.

†To whom correspondence should be addressed. E-mail: ckenyon@biochem.ucsf.edu